Available online at www.sciencedirect.com
SCIENCE DIRECT
Catalysis Today 105 (2005) 589–597
CATALYSIS TODAY
www.elsevier.com/locate/cattod

Positioning of the reaction zone for gas–liquid reactions in catalytic membrane reactor by coupling results of mass transport and chemical reaction study

Gorazd Berčič *, Albin Pintar, Janez Levec

Laboratory for Catalysis and Chemical Reaction Engineering, National Institute of Chemistry, P.O. Box 660, SI-1001 Ljubljana, Slovenia

Abstract

The location of the reaction zone in the catalytic membrane contactor was determined for two-phase reaction system. As a model reaction oxidation of formic acid by Pt catalyst deposited in the ceramic membrane filtration layer was used. It was determined from gas–liquid mass transport experiments that at gas side overpressures from 0.5 to 0.9 bar the liquid was displaced from membrane support layer and that the tortuosity factor of membrane filtration layer is 3.1. It was estimated on the basis of CO_2 fluxes that the reaction zone is close to gas–liquid interface and that the locus of the reaction zone matches with O_2 penetration depth calculated on the basis of formic acid disappearance rate. It was also shown that partition coefficient of formic acid in the membrane filtration layer is higher than 1, otherwise formic acid could not migrate to the reaction zone. Only a small fraction of the catalyst was involved in the reaction. The apparent activation energy was estimated to be around 44 kJ/mol.

Keywords: Membrane reactor; Catalysis; Formic acid oxidation; Reaction zone; Partition coefficient

1. Introduction

In the last years, catalytic membrane reactors (CMR) operated under contactor mode, as described by Mota et al. [1], attained great interest for industrialization due to unique possibility to contact gaseous and liquid reactants without prior mixing directly on the catalyst. Since the catalyst is fixed in the membrane support, further separation steps, which are necessary when slurry reactors are used, are not required. In the two EU research projects under FP5, the potentials of catalytic membrane reactors are studied in order: (a) to gain productivity and selectivity of hydrogenation processes [2] and (b) to examine possibility to replace classic wet air oxidation (WAO) reactors which operate under severe conditions, with a membrane contactor as a catalytic wet air oxidation (CWAO) reactor which could operate at mild operation conditions [3]. This technology, if applicable, will lower the operating costs and extend the range of construction materials, since ordinary construction materials could be used.

It has been already mentioned by Cini and Harold [4] that it is theoretically possible to establish an idealized situation, where reactants contact directly in the catalytic region in the membrane reactors by proper adjustment of operation conditions. The concept of CMR reactor was mainly studied with hydrogenation reactions. Peureux et al. [5] studied hydrogenation of nitrobenzene, but they did not observe significant increase of reactor productivity when they reversed the sides for gas and liquid feed to the membrane contactor. Reif and Dittmeyer [6] suggested that for the case when internal diffusion in CMR is a rate determining step, the reactor productivity could be increased by pumping reaction mixture with the dissolved reactant through the membrane; they reported that such operation can increase reactor productivity up to five times. Vospernik et al. [7] showed that it is possible to control position of gas–liquid interface inside the membrane wall by applying different

* Corresponding author. Tel.: +386 1 47 60 282; fax: +386 1 47 60 300.
E-mail address: gorazd.bercic@ki.si (G. Berčič).

0920-5861/$ – see front matter © 2005 Elsevier B.V. All rights reserved.
doi:10.1016/j.cattod.2005.06.008

Nomenclature

a	membrane inner surface area (m^2)
A	pre-exponential factor in Eq. (13)
C	concentration (mol/m^3)
d_{CO_2}	diffusion path of CO_2 in planar geometry (m)
D	diffusion coefficient (m^2/s)
E_a	activation energy (kJ/mol)
H	Henry's law constant
k	mass transfer coefficient (m/s)
K_L	overall mass transport coefficient (m/s)
K_{ads}	adsorption constant in Eq. (13) (L/mol)
l	diffusion path in planar geometry (m)
N	molar flow (mol/s)
p_1–p_6	parameters in Eqs. (4) (5)
$(-r_i)$	reaction rate (mol/s)
r	radius of membrane channel (m)
r^{GL}	radius of gas–liquid interface (m)
r^{RZ}	location of reaction zone (m)
R	radius of membrane (m)
R_g	universal gas constant (8.314 J/(mol K))
t	time (s)
T	temperature (K)
V	tank volume (m^3)

Subscripts/superscripts

app	apparent
CO_2	carbon dioxide
G	gas
GL	at gas–liquid interface
GS	to the gas side
HCOOH	formic acid
LS	to the liquid side
L	liquid
N_2	nitrogen
O_2	oxygen
ref	as a reference
RZ	at reaction zone
t	theoretical value

Greek letters

ε	porosity
τ	tortuosity factor

trans-membrane pressure. By proper adjustment of trans-membrane pressure, it was possible to increase mass transport through the membrane for more than 20 times compared to liquid full operation. Productivity of CMR for the case of hydrogenation reaction can be further increased by enlarging mass transfer coefficient by insertion of static mixers in the membrane channel [8]. However, during the oxidation of formic acid such enlargement of external mass transport did not increase reactor productivity [9]. Recently, Iojoiu et al. [10] showed that gas–liquid interface could be pushed from the first intermediate layer toward the top layer, which resulted in increased reactor productivity which was proportional to the ratio of intermediate layers thicknesses. They reported that there was no remarkable difference in reactor productivity when air was used instead of O_2. In addition to the non-consistencies observed during enlargement of external mass transport and minimal influence of oxygen partial pressure on observed CMR productivity, a question remains how the amount of catalyst and catalyst distribution influence the reactor productivity, since similar activities were reported for membranes made of different materials having different thickness of filtration layers and different catalyst loadings [9,10]. The main aim of this study was to determine the location of reaction zone (RZ) in the CMR. For this purpose, the results of mass transport study (CO_2) were combined with the results of catalytic oxidation of formic acid. All experiments were carried out under the same operating/reaction conditions. The key idea of this work was to correlate the fluxes of CO_2 measured during the reaction by means of appropriate mass transport correlation, which was derived on the basis of CO_2 mass transport experiments performed in the absence of reaction. Since the operating conditions were equal in both cases, the physical situation within the membrane wall should be the same also under the oxidation tests. Therefore, it would be possible to estimate the location of RZ based on calculated CO_2 fluxes from the RZ toward the gas and liquid side.

2. Experimental

2.1. Ceramic membranes

As a catalyst support ceramic membranes supplied by Pall Exekia (Bazet, France) were used. Membranes were tubular (o.d. 10 mm) multi layered 250 mm long pieces. The membrane support layer and the first two filtration layers were made of α-Al_2O_3 particles coated by TiO_2. The average pore diameter of support was 12 μm (thickness 1.5 mm), while the average pore diameter of first and second intermediate layers were 0.8 and 0.2 μm (thickness 20 and 17 μm, respectively). The 5 μm thick top layer was made of ZrO_2 particles and had 20 nm pore size. Membranes were enamelled at both ends to assure appropriate surface for sealing with O-rings.

2.2. Catalytic membrane preparation and characterization

For membrane impregnation, an adopted procedure disclosed by Fehn et al. [11] in the US Patent 5,531,181 was used. As a Pt precursor H_2PtCl_6 (Sterm Chemicals, 39.85% Pt) was used. 0.2 mL of high concentrated Pt solution (50 g Pt/L for 10 mg Pt loading and 5 g Pt/L for 1 mg Pt loading) was spread over the inner filtration layer of the membrane. Following the impregnation, membranes

were left overnight in vertical position. Impregnated membranes were put into the tunnel oven and dried in the N_2 atmosphere (50 mL/min) slowly (1 K/min) up to 358 K. After 40 min, temperature was increased to 378 K (1.5 K/min). After 60 min of drying, the sample was heated up to 573 K (1 K/min). At 573 K, the gas flow was switched to hydrogen (50 mL/min) for 120 min in order to reduce Pt species to metal Pt nanoparticles. The membrane was cooled down overnight under N_2 atmosphere.

After experiments the membrane with 10 mg Pt loading was crushed and sent to scanning electron microscope and electron probe microanalysis in order to obtain the information about Pt distribution in the prepared catalytic membranes. Detailed information about analysis could be found elsewhere [9]. The results in the form of SEM–BSE cross-section images and EPMA analysis are shown in Fig. 1. It is evident that Pt is highly concentrated in the top filtration layer, while the Pt signal in the supported layers is hidden in a baseline noise. The concentration of Pt in these layers is also under the detection limit of EPMA analysis. However, visual observations inspired us to take also pictures by digital camera and ordinary reflected light microscope. From the digital photography (Fig. 2a), which shows membrane cross-section, it is clear that the precursor solution during impregnation process reached also intermediate and support layers, since they are noticeably colored by Pt particles. In Fig. 2c, we can see that the amount of deposited Pt decreases in direction towards external intermediate layers. It is evident from Fig. 2a that the impregnation solution did not completely wet the support layer.

2.3. Experimental set-up

Experimental apparatus is schematically shown in Fig. 3, while experimental conditions are summarized in Table 1. Gas lining is shown in dark grey color, while liquid piping is drawn with the black lines. Prior to each experiment, liquid circuit was flushed three times and then filled with distilled

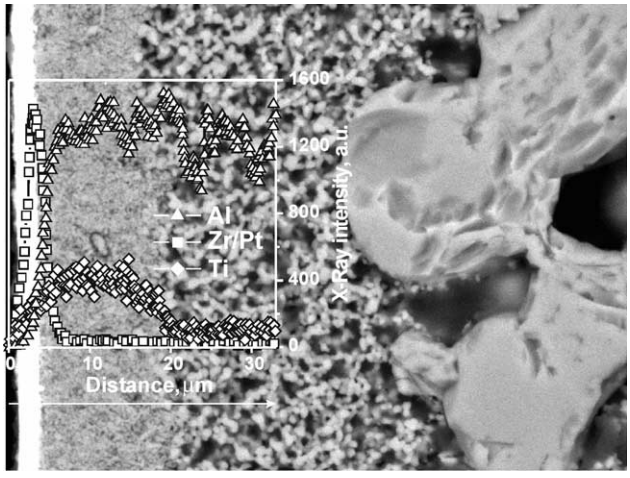

Fig. 1. Results of EPMA analysis superimposed on the SEM/BSE image of membrane loaded with 10 mg Pt.

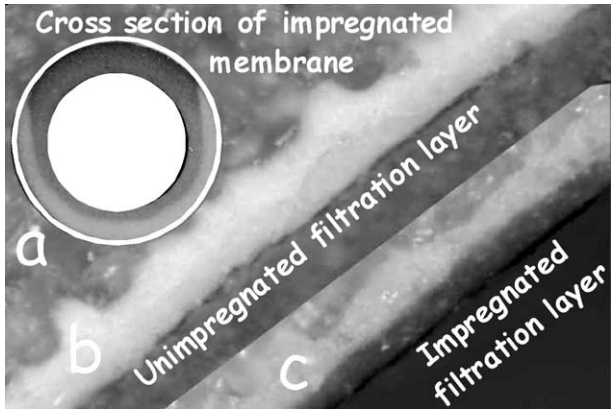

Fig. 2. Photos of membrane cross section (10 mg Pt loading) taken by digital camera (a), and cross section of filtration layer before (b) and after (c) impregnation as viewed by reflected light microscope.

water. Water was then slowly led into the gas compartment of reactor assembly through the gas side draining valve (11) in order to assure complete wetting of membrane. When experiments were started the pressure on the gas side first increased to 50 mm H_2O and then water was slowly drained out of the gas compartment. Gas overpressure was applied in order to prevent water inflow into the gas compartment of reactor assembly. The level of water in the graduated burette, which was used to measure the volume of displaced liquid from the membrane wall and for detection of leaking, when gas overpressure was applied, was adjusted to the starting position by opening the liquid drain valve (12).

Then the pressure increased to the desired value by regulating solenoid valve (13) and temperature of the thermostat and water in the CSTR were adjusted. Operation of experimental apparatus was controlled by a computer

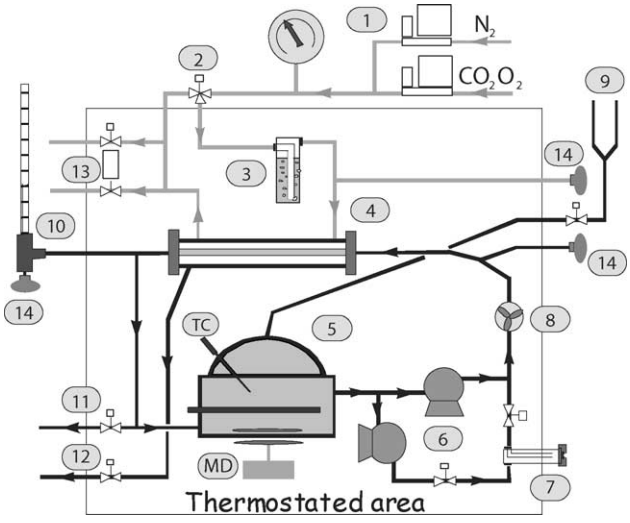

Fig. 3. Schematic representation of apparatus used in this study: (1) electronic mass flow controllers, (2) three port valve, (3) gas saturation unit, (4) membrane reactor assembly, (5) reservoir/CSTR tank, (6) gear pump, (7) sampling port, (8) liquid flow meter, (9) reactant injection port, (10) graduated burette, (11 and 12) drain valves, (13) regulating solenoid valve, (14) differential pressure transducers.

Table 1
Experimental conditions

Operating temperature (K)	308, 318, 328
Trans-membrane pressure (bar)	0.5, 0.717, 0.926
Reactor volume (mL)	343
Gas flow rate (mL/min)	40
Liquid flow rate (mL/min)	360
Initial concentration of formic acid (g/L)	2.13
Catalyst loading (mg Pt/membrane)	1, 10
CO_2 mol fraction in the gas phase for mass transport study	0.125, 0.165, 0.218
Oxidation gas	O_2
Membrane porosity	0.39
Membrane o.d. (mm)	10
Membrane i.d. (mm)	7

connected to microprocessor controlling unit, which regulated, measured and adjusted all devices and sensors used in the apparatus. Once operating conditions were reached, the small amount of concentrated formic acid (0.6 mL) was injected in the apparatus through the liquid injection port (9). With 10 mL of additional water injected through the same port the formic acid was flushed into the reactor. After 3 min, nitrogen flow was replaced by oxygen and three-port reactor bypass valve (2) was opened in order to flush N_2 from the piping. After additional 2 min, the three-port reactor bypass valve was closed and O_2 was directed through the gas saturation unit (3) to membrane reactor (4). This time was taken into account in our analysis as the time zero. Samples were taken periodically from the reactor through syringe sampler (7). The protocol used during mass transport studies was identical, only acid injection procedure was skipped. Pressure in the reactor was measured by differential pressure transducers (Motorola, models MPX5700, MPXV5004 and MPX51000). Gas flow was regulated by electronic mass flow controllers (Sensirion, model PC1_L6U1V_1N), and liquid flow rate was measured by turbine flow sensor (EQUFLOW, model 0045.T.N.T.). The flow was regulated by varying power applied to simple gear pumps (B&D Pumps, model UGP-2000). Pressure in the system was regulated by means of solenoid valve (Aalborg, PVS-2) connected to the microprocessor unit. Liquid in the tank (5) was mixed by a magnet drive (MD); temperature control was performed by measuring temperature by K-type thermocouple (TC) and applying appropriate power to 200 W electrical heater. Fuzzy logic controlling algorithm was used for adjusting temperature and pressure in the reactor system. Parts used for reactor construction were inert and did not contribute to the reaction, since no conversion was observed during blank tests carried out with the non-impregnated membrane. All crucial parts of apparatus used in this study were placed in the thermostat in order to assure temperature stability and prevent condensation on the housing of gas compartment and in the piping used for gas phase. Apparatus was designed to operate up to 333 K and 1 bar gas overpressure. Main construction parts were made of SS, polymethylmethacrilate and polyethylene.

All catalytic tests were performed with the same initial concentration of formic acid. Concentrated formic acid with a volume of 0.6 mL was dosed into the CSTR (~2.13 g/L, initial TOC ~ 556 mg C/L). Analyses of liquid samples were performed by means of a TOC Analyzer (Rosemount/Dohrmann, model DC-190). CO_2/N_2 gas mixture was prepared by adjusting flow rates of corresponding flow controllers. Concentration of CO_2 in the gas mixture was determined by IR gas analyzer (Edinburgh Instruments, model Gas Card II).

3. Results and discussion

3.1. Mass transport validation

Mass transport was studied with gas mixtures of CO_2 and N_2. Carbon dioxide was produced during the oxidation of formic acid somewhere in the wetted part of membrane. Because at the beginning of experiment gas and liquid phase were low in CO_2 content, CO_2 diffused from the reaction zone in both directions, i.e. in the gas and liquid phase. Therefore, all uncertainties in predicted values of physical properties and saturation concentration have the same effect on predicted profiles of CO_2 during reaction and non-reaction conditions. By selecting CO_2 for mass transport studies, the systematic error was minimized, since it is not necessary that differences between real values of physical parameters and estimated ones with an appropriate correlation are of the same value and sign when two different gases are used. Mass transport of CO_2 across the membrane wall can be expressed as follows:

$$N_{CO_2} = K_{CO_2} a^{ref} (C^{G}_{CO_2} - C^{L}_{CO_2}) \quad (1)$$

where coefficient K is overall mass transport coefficient and is defined for cylindrical geometry analogously to heat transfer through the insulated tube [12], when inner membrane wall surface is taken as a reference surface, by the following equation:

$$\frac{1}{K_{CO_2}} = \frac{H^{app} r}{k^{G}_{CO_2} R} + \frac{\tau H^{app} r}{\varepsilon D^{G}_{CO_2}} \ln\left(\frac{R}{r^{GL}}\right) + \frac{\tau r}{\varepsilon D^{L}_{CO_2}} \ln\left(\frac{r^{GL}}{r}\right) + \frac{1}{k^{L}_{CO_2}} \quad (2)$$

The first term on the right side of Eq. (2) represents mass transport resistance on the gas side and is small compared to the values of other terms; therefore, it was omitted in further analyses. The second term stands for diffusion of gaseous CO_2 through the ''dry'' part of membrane wall. The Fick's law was used for prediction of mass transport inside the membrane wall. The apparent Henry's constant was introduced for conversion from gas concentration units to liquid concentrations units. The third term represents diffusion through the wetted part of membrane wall, while

the last term accounts for mass transfer from the main liquid to the membrane wall. Diffusion coefficients of components in gas phase were calculated from the correlation proposed by Fuller et al. [13], while diffusivity of formic acid in the liquid was calculated using the Hayduk–Minhas correlation, and Wilke–Chang [13] correlation was used for prediction of diffusion coefficients of oxygen and carbon dioxide. Mass transfer coefficient in the liquid phase was calculated from the correlation for laminar flow through a tube [14]. Numerical values of apparent Henry's law constants were calculated from gas phase concentrations and the corresponding equilibrium concentrations in the liquid phase from the correlation proposed in [15]. Numerical values are summarized in Table 2.

The position of gas–liquid interface in the membrane wall was calculated by fitting experimentally measured concentration in the CSTR with the following model:

$$V\frac{dC}{dt} = K_{CO_2}a(C^{G}_{CO_2} - C^{L}_{CO_2}) \quad (3)$$

Since the unknown parameters are coupled in constant K_{CO_2}, it was not possible to separate them, therefore it was decided that values of tortuosity factor will be calculated for various penetration depths of gas–liquid interface. It was assumed that position of gas–liquid interface matches with the position of intermediate layers. From our previous research [7] it was clear that the trans-membrane pressure (TMP) of 0.35 bar is sufficient to push gas–liquid interface next to the first intermediate (filtration) layer. The interface remains at this location until TMP has increased above 4 bar [10]. Since we operated in the TMP range from 0.5 to 0.92 bar, the position of gas–liquid interface should be fixed at the same location for all our experiments. Validity of this assumption could be confirmed if the derived mass transfer model successfully predicted experimentally measured curves. By means of non-linear regression programme, where fifth order Cash-Kerp Runge Kutta integration algorithm [16] was used for the integration of Eq. (3), and by means of Marquart minimization algorithm [17] used for determination of optimal value of tortuosity factor from Eq. (2), the optimal values of tortuosity factor were determined for different positions of gas–liquid interface. In Fig. 4, a comparison between predicted and experimentally measured concentration profiles is shown. It is evident that the agreement is very good. This confirms the above-described hypothesis about stable and fixed position of gas–liquid interface in the whole range of experimental conditions employed. From Fig. 1, the diffusion depth for wetted part of membrane was estimated as follows: first intermediate layer $r^{GL} - r = 50$ μm, second intermediate layer $r^{GL} - r = 20$μm, and finally top filtration layer $r^{GL} - r = 4$ μm. After minimization, the following values of corresponding tortuosity factors were obtained: 3.1, 7.6 and 48.4, respectively. The first value seems to be most probable when compared with the published data [18]. We have to stress that constant porosity was assumed for all layers. From gas permeability experiments Kikkinides et al. [19] showed that porosity of intermediate layers does not considerably differ from that of support layer. In Fig. 1, we can see that at the contact of two layers there is a region of reduced porosity, since smaller particles enter into larger pores of neighboring layer. If we assume that the thickness of the region with reduced porosity is 5 μm, and that reduced porosity is 0.152 (0.39 × 0.39), then for the diffusion length of 50 μm we obtain numerical value of 2.6 for tortuosity factor, which is even more realistic according to literature data [18]. However, in further analysis the value of 3.1 was used to avoid introduction of unknown parameters. It should be noted that the relative position of RZ inside the wetted part of membrane wall is independent of the product $\tau(r^{GL} - r)$, since RZ is located within the "diffusion path" region determined from mass transport experiments.

Table 2
Numerical values of physical properties

Physical property	Temperature (K)		
	308	318	328
Liquid phase			
HCOOH			
$k_L \times 10^5$ (m/s)	1.13	1.31	1.50
$D \times 10^9$ (m^2/s)	1.93	2.40	2.93
CO_2			
$k_L \times 10^5$ (m/s)	1.37	1.59	1.82
$D \times 10^9$ (m^2/s)	2.58	3.21	3.92
O_2			
$D \times 10^9$ (m^2/s)	3.01	3.75	4.58
Gas phase			
O_2			
H	0.0276	0.0254	0.024
CO_2			
D (P = 1.5 bar) × 10^5 (m^2/s)	1.18	1.25	1.32
D (P = 1.717 bar) × 10^5 (m^2/s)	–	1.09	–
D (P = 1.926 bar) × 10^5 (m^2/s)	–	–	1.03
H	0.665	0.554	0.477

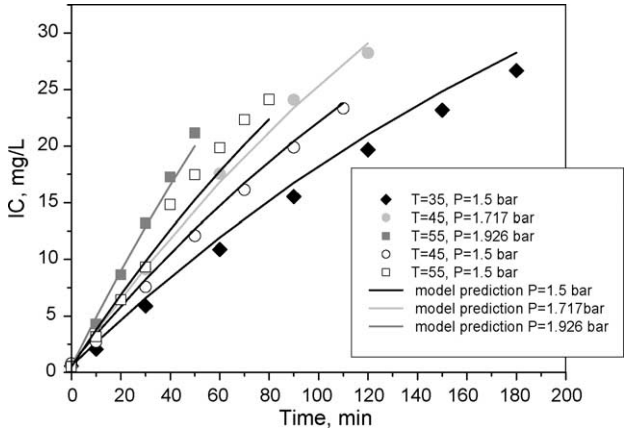

Fig. 4. Comparison between predicted and experimentally measured amounts of dissolved CO_2 in reservoir during mass transport study.

3.2. Reaction zone determination from formic acid oxidation experiments

Oxidation of formic acid was performed in the temperature range from 308 to 328 K and at three different gas overpressures namely 0.5, 0.717 and 0.926 bar, while the liquid side was opened to the atmosphere. Initial concentration of formic acid was approximately 2.13 g/L, which corresponds to 556 mg C/L. In the selected pressure range, the equilibrium concentrations of oxygen in the liquid phase were equal, despite different temperatures, which enabled us to calculate apparent activation energy, as it is explained below.

Since our main interest was the calculation of fluxes from and to the reaction zone, we decided to calculate concentration derivatives numerically rather than analytically from discrete values. For this purpose, coefficients of appropriate smooth continuous functions:

$$\frac{dC_{TOC}}{dt} = -p_1 C_{TOC}^{p_2}, \quad C_{TOC} = p_3 \text{ at } t = 0 \tag{4}$$

for TOC curves and

$$\frac{dC_{IC}}{dt} = -p_4(p_5 - C_{IC}), \quad C_{IC} = p_6 \text{ at } t = 0 \tag{5}$$

for IC curves were calculated numerically for each experimental data set separately. From results shown in Fig. 5 we can see that approximation functions match experimental data very well and therefore could be used in further analysis for calculation of desired fluxes. Numerical values of coefficients in approximation functions are not listed here, since they have no physical meaning. As it was already mentioned, the location of RZ was estimated on the basis of CO_2

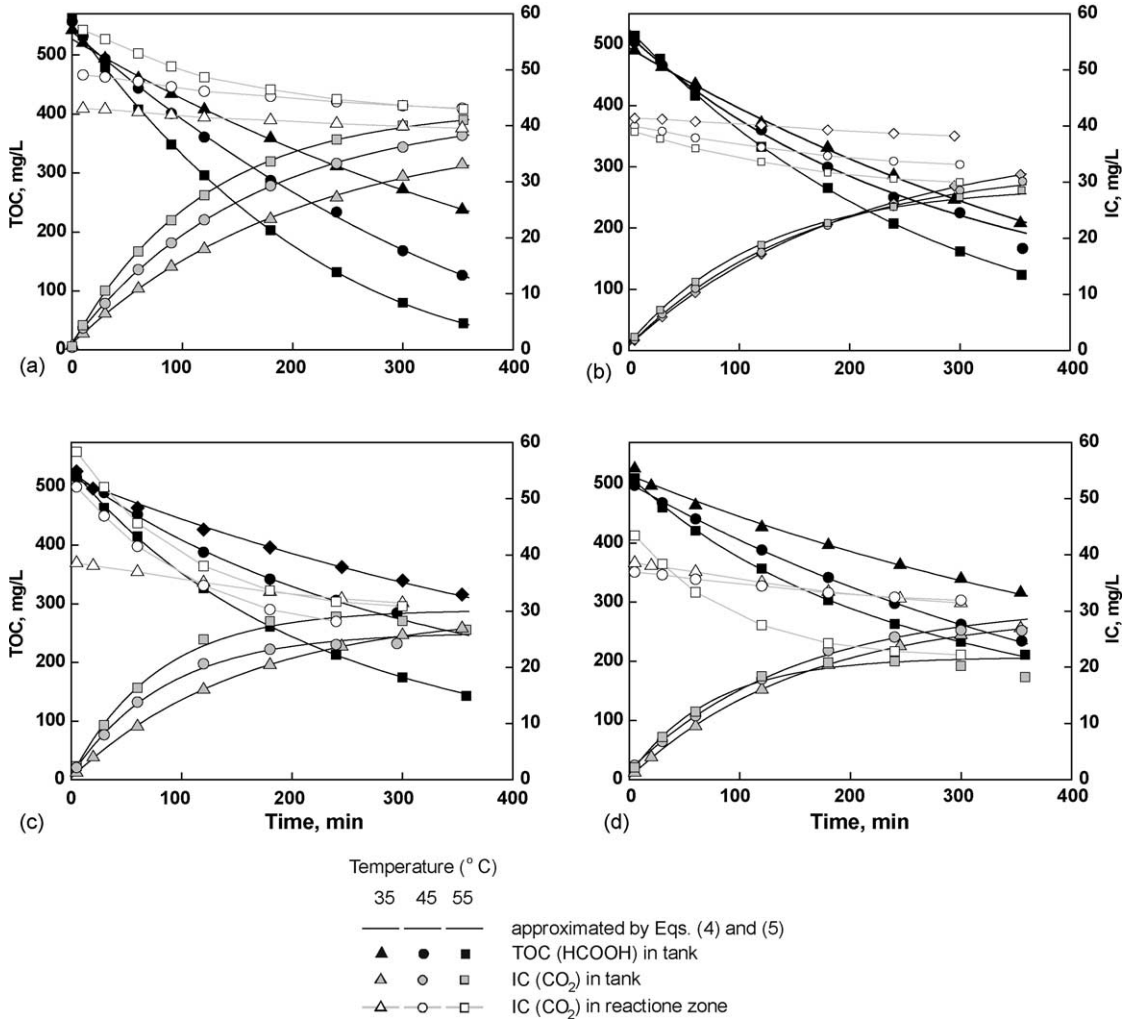

Fig. 5. Experimentally measured course of formic acid oxidation at conditions of constant trans-membrane pressure of 0.5 bar (b and d) and at constant (1.57 mol/m^3) concentration of dissolved O_2 (a and c) obtained with two different membranes having 10 mg Pt (a and b) and 1 mg Pt (c and d) loading.

fluxes. Despite non-steady state conditions during the reaction we assumed quasi steady state in order to simplify our estimation. Since the reaction was relatively slow and the volume of liquid in membrane pores was negligible compared to the total amount of liquid, this assumption is acceptable and certainly will not influence correctness of predictions and conclusions drawn from derived observations.

We assume that the reaction zone is infinitesimal. The amount of CO_2 released during formic acid oxidation is equal to formic acid flow to the reaction zone, which is proportional to the slope of TOC curve and was calculated from the approximation functions:

$$N^{RZ}_{CO_2} = N_{HCOOH} \propto -\frac{dC_{TOC}}{dt} \tag{6}$$

The molar flow of CO_2 from RZ to liquid side is proportional to the slope of IC curve:

$$N^{LS}_{CO_2} \propto \frac{dC_{IC}}{dt} \tag{7}$$

while the molar flow of CO_2 to the gas side is proportional to the difference between slopes of TOC in IC curves:

$$N^{GS}_{CO_2} \propto \left(-\frac{dC_{TOC}}{dt} - \frac{dC_{IC}}{dt} \right) \tag{8}$$

To determine the location of RZ, the set of following two equations must be solved:

$$0 = N^{GS}_{CO_2} - \frac{\varepsilon D^{L}_{CO_2}}{\tau} a \frac{(C^{RZ}_{CO_2} - C^{GL}_{CO_2})}{d_{CO_2} - l^{RZ}} \tag{9}$$

$$0 = N^{LS}_{CO_2} - \frac{1}{\frac{\tau(l^{RZ}-0)}{\varepsilon D^{L}_{CO_2}} + \frac{1}{k_L}} a (C^{RZ}_{CO_2} - C^{L}_{CO_2}) \tag{10}$$

The above two equations are written for planar geometry. Since previously determined thickness of wetted membrane layers from CO_2 mass transport experiments was only 50 μm, this assumption is not critical since membrane I.D. is about 140 times larger than the estimated diffusion path. Due to planar transformation the previously determined diffusion path ($r^{GL} - r$) was replaced by d_{CO_2} and the coordinate system was relocated from the center of membrane channel to the membrane wall. The concentration of $C^{GL}_{CO_2}$ was determined from the gas flow rate and CO_2 molar flow to the gas side. In calculation, we used average concentration of CO_2, since plug flow was assumed in the gas compartment of membrane contactor. The system of Eqs. (9) and (10) was solved using LMNLE subroutine from BNALib [20] for solving non-linear equations based on Lavenberg–Marguardt method. As a result, we obtained concentration of dissolved CO_2 in the reaction zone and the locus of reaction zone. Calculated values of $C^{RZ}_{CO_2}$ are shown together with the experimentally measured values in the CSTR in Fig. 5. In Fig. 6, the locus of reaction zones are shown by black symbols connected by lines. In the same figures, theoretical diffusion depths of reactants for measured reaction rates are also shown for both oxygen and formic acid; for the case of formic acid we also demonstrate how 10-fold increase of external mass transport coefficient k_L influences the penetration locus of formic acid. The penetration depth of oxygen was calculated by means of Eq. (9), where we accounted for reaction stoichiometry, use of oxygen properties and concentrations. For oxygen the equation has the following form:

$$d_{CO_2} - l_{O_2} = \frac{\varepsilon D^{L}_{O_2}}{\tau} a \frac{C^{GL}_{O_2}}{0.5 N_{HCOOH}} \tag{11}$$

Since pure oxygen was used, $C^{GL}_{O_2}$ was assumed to be equal to O_2 equilibrium concentration for particular experimental conditions. Similarly, the diffusion depth of formic acid was calculated from Eq. (10) as follows:

$$l_{HCOOH} = \left(\frac{a C_{HCOOH}}{N_{HCOOH}} - \frac{1}{k^{HCOOH}_{L}} \right) \frac{\varepsilon D^{L}_{HCOOH}}{\tau} \tag{12}$$

From results presented in Fig. 6, we can see that O_2 penetration depth overlaps with the calculated locus of reaction zone predicted from CO_2 molar flows over the whole range of experimental conditions used. It is obvious from this fact that the reaction zone is determined by oxygen mass transport to the catalyst, and that the concentration of catalyst at this location is sufficient for reaction, or even more probably that Pt impregnation extends to this location. From the calculated penetration depths of formic acid in membranes loaded with 1 mg of Pt (Fig. 6c and d) we can conclude that supply of formic acid by mass transport is sufficient, since formic acid theoretically could diffuse deeper into the membrane wall, certainly if the membrane wall is wet. More interesting are results shown in Fig. 6a. We can see that only at the beginning of experiments sufficient amount of formic acid could be supplied to the reaction zone. In the further stage of reaction, the difference between penetration depth of formic acid and location of reaction zone, calculated from either CO_2 molar flows or from O_2 penetration locus, increases and therefore, according to our previous assumption, reaction could not take place at such rate. Since we measured higher reaction rates than are possible by means of ordinary diffusion, the actual molar flow must have been enlarged by other phenomena. One of the most possible explanations for this is that partition coefficient of formic acid is higher than 1 in the system formic acid–membrane filtration layer. So far, this was observed mostly with polymeric and organic membranes and it was not mentioned in connection with the ceramic filtration membranes.

The actual concentration profile of formic acid is supposed to look like it is shown schematically in Fig. 7, where concentration profiles for mass transport across a polymeric membrane are also shown. It is obvious that mass transport of formic acid is increased due to the high partition coefficient of formic acid. Actually, the penetration depth of

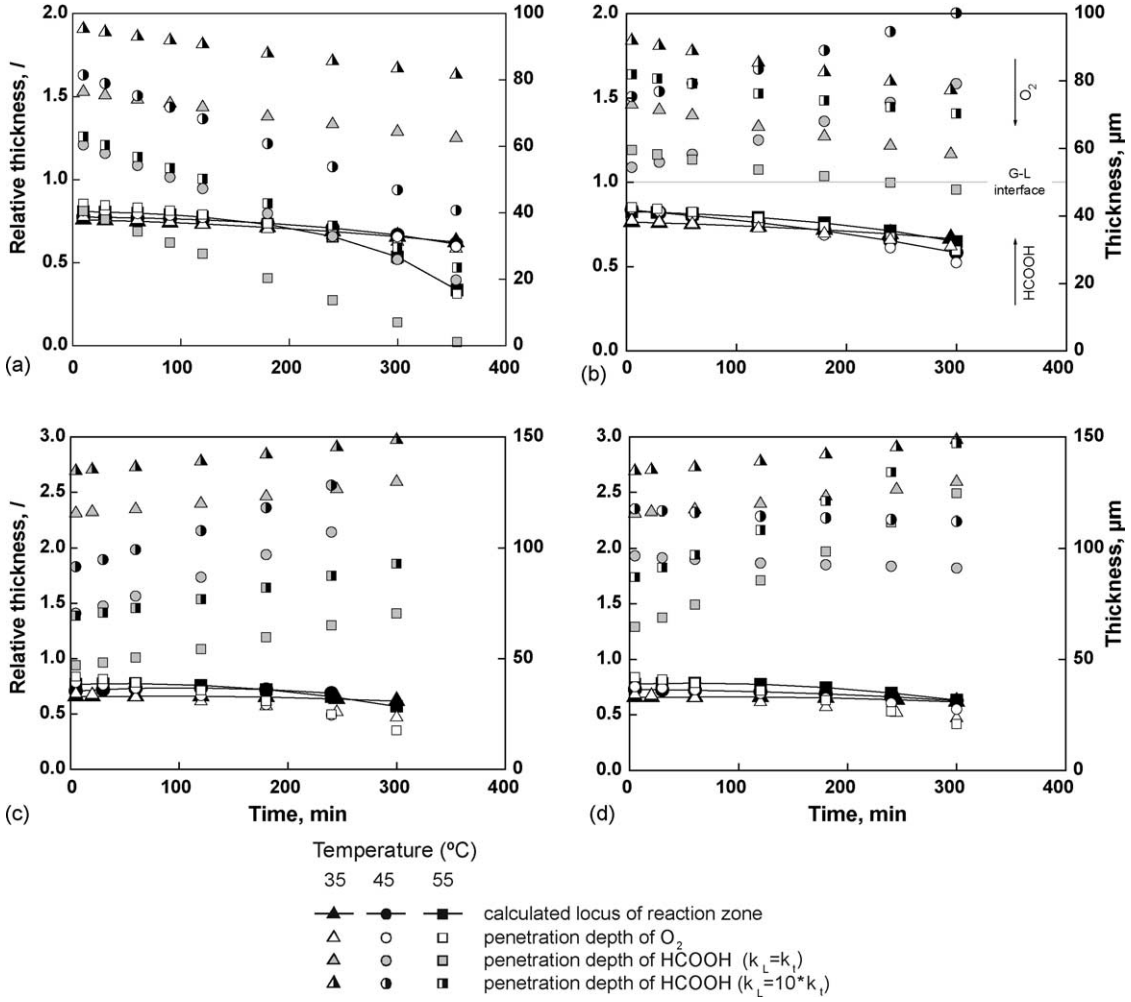

Fig. 6. Comparison between predicted location of reaction zone on the basis of CO_2 fluxes and calculated one from experimentally determined fluxes of oxygen and formic acid. Graphs are arranged in the same order as in Fig. 5. The position of gas–liquid interface is shown in graph (b) and corresponds to ordinate value of 1 (50 μm).

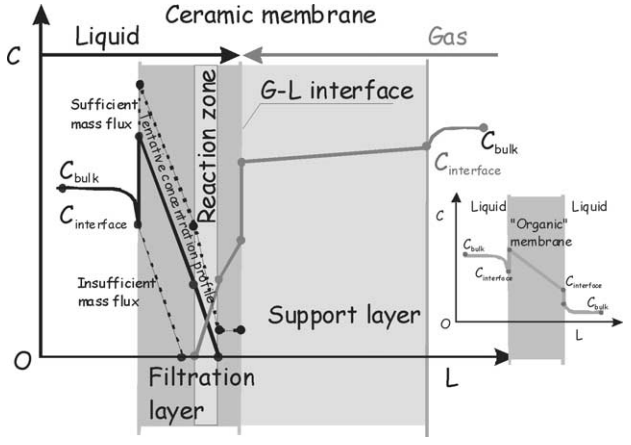

Fig. 7. Comparison between concentration profiles during mass transport through the polymeric membrane and tentative concentration profile of formic acid, which formed in the filtration layer of ceramic membrane during HCOOH oxidation.

formic acid is much longer than the one presented in Fig. 6 due to partition coefficient. We can not state how concentration influences the partition coefficient, but from the analysis of ordinary diffusion through the membrane wall at low HCOOH concentrations (for the time of 300 and 360 min) we can conclude that partition coefficient could be greater than 10. High partition coefficient of formic acid could be also the main reason why Vospernik et al. [9] found the same reactor activity during the oxidation of formic acid despite the increase of external mass transport by means of varying recirculation rate and by insertion of static mixers. It is also possible that high partition coefficient causes comparable reactor productivities reported by Iojoiu et al. [10] for membranes having different composition, thickness of filtration layers and Pt loading.

From the slopes of experimental curves measured at ‘‘constant’’ oxygen concentration we estimated also the apparent activation energy. For the case of equal instanta-

neous reactant concentrations in the bulk liquid phase, the generalized reaction rate expression could be simplified to:

$$(-r_{\mathrm{HCOOH}}) = A\,\mathrm{e}^{-E_a/RT}\, f(C_i, K_{\mathrm{ads},i}) \quad (13)$$

If we further assume that in the examined temperature range adsorption constants are not strong functions of temperature, then the above equation could be rearranged to:

$$\ln(-r_{\mathrm{HCOOH}}) = \ln(A) - \frac{E_a}{RT} + \ln(\, f(C_i, K_{\mathrm{ads},i})) \quad (14)$$

from which we can estimate the value of apparent activation energy if we plot $\ln(-r_{\mathrm{HCOOH}})$ versus $1/T$ for experimental data measured at the same formic acid concentration and constant oxygen concentration. From these plots, we estimated value of E_a for both membranes used in this study. The plots showed linear dependency and therefore, we can conclude [21] that external diffusion did not influence measured reaction rates. We found out that the value of apparent activation energy increases with a decrease of formic acid concentration. In the corresponding range of TOC concentrations from 500 to 300 mg C/L, the average value of E_a for 10 mg Pt loading was about 37 kJ/mol (11% deviation in concentration range from 500 to 300 mg C/L) and 44 kJ/mol (3% deviation) for 1 mg Pt loading. It is obvious that despite high partition coefficient of formic acid, mass transport resistances are still present in the membrane wall. Global reaction rate is lower for low Pt loading, which is showed by shifting the reaction zone towards the liquid side. This also causes that concentration of formic acid in the reaction zone is higher. When we compare values of apparent activation energy with the literature reported data of 47.6 kJ/mol [22], we find out that the values are very close despite the fact that Harmsen et al. [22] studied liquid phase oxidation of formic acid in the slurry reactor at lower temperatures (282–293 K) and with a different catalyst, i.e. carbon powder loaded with 1% of Pt.

4. Conclusions

In this study, we established that the partition coefficient of formic acid in the membrane filtration layer is higher than 1 and that only a fraction of deposited catalyst was involved in the reaction. These findings can be crucial for the design and evaluation of ceramic membrane reactors, since the catalyst loading can be reduced, if intermediate layers could be selectively impregnated. Since the mass flux from the liquid side is enlarged due to high partition coefficient, the activity of membranes is much higher than it was assumed till now. It should be established by additional investigations if formic acid is an exception or high partition coefficients will be observed also in/with other substances and other ceramic membranes.

Acknowledgements

The authors gratefully acknowledge the financial support of Slovenian Ministry of Education, Science and Technology (program no. P2-152) and European Commission (Watercatox Project, contract no. EVK1-CT-2000-00073).

References

[1] S. Mota, S. Miachon, J.-C. Volta, J.-A. Dalmon, Catal. Today 67 (2001) 169.
[2] http://www.leia.es/Camertoil/public.html.
[3] http://www.sintef.no/watercatox.
[4] P. Cini, M.O. Harold, AIChE J. 37 (1991) 997.
[5] J. Peureux, M. Torres, H. Mozzanega, A. Giroir-Fendler, J.-A. Dalmon, Catal. Today 25 (1995) 409.
[6] M. Reif, R. Dittmeyer, Catal. Today 82 (2003) 3.
[7] M. Vospernik, A. Pintar, G. Berčič, J. Levec, J. Membr. Sci. 223 (2003) 157.
[8] M. Vospernik, A. Pintar, G. Berčič, J. Batista, J. Levec, Chem. Eng. Res. Des. 82 (2004) 659.
[9] M. Vospernik, A. Pintar, G. Berčič, J. Levec, J. Walmsley, H. Raeder, E.E. Iojoiu, S. Miachon, J.-A. Dalmon, Chem. Eng. Sci. 59 (2004) 5363.
[10] E.E. Iojoiu, J.C. Walmsley, H. Raeder, S. Miachon, J.-A. Dalmon, Catal. Today 104 (2005) 329.
[11] E. Fehn, F. Schmid, J. Plesow, US Patent 5,543,181 (1996).
[12] J.P. Holman, Heat Transfer, McGraw-Hill, 1986,, p. 35.
[13] B.E. Poling, J.M. Prausnitz, J.P. O'Connell, The Properties of Gases and Liquids, fifth ed., McGraw-Hill, 2001, p. 11.21.
[14] E.L. Cussler, Diffusion: Mass Transfer in Fluid Systems, second ed., Cambridge University Press, 1999,, p. 227.
[15] P.G.T. Fogg, W. Ferrand, Solubility of Gases in Liquids, Wiley, 1990.
[16] W.H. Press, S.A. Teukolsky, W.T. Vettering, B.O. Flanney, Numerical Recipes in Fortran, second ed., Cambridge University Press, 1992, p. 173.
[17] R.G. Duggleby, Comput. Biol. Med. 14 (1984) 447–455.
[18] N.C. Satterfield, Mass Transfer in Heterogeneous Catalysis, MIT Press, 1970,, p. 58.
[19] E.S. Kikkinides, K.A. Stoitsas, V.T. Zaspalis, V.N. Burganos, J. Membr. Sci. 243 (2004) 133.
[20] C.D. Eagel, BNALib—A Basic Nonlinear Analysis Library for Personal Computers, http://cdeagle.cnchost.com.
[21] H.S. Fogler, Elements of Chemical Reaction Engineering, Prentice-Hall, 1986,, p. 587.
[22] J.M.A. Harmsen, L. Jelemensky, J.P.M. van Andel-Scheffer, B.F.M. Kuster, G.B. Marin, Appl. Catal. A 165 (1997) 499.